Author Manuscript

Author Manuscript

Author Manuscript

Author Manuscript

HHS Public Access

Author manuscript

Proc IEEE Int Symp Biomed Imaging. Author manuscript; available in PMC 2021 September 20.

Published in final edited form as:

Proc IEEE Int Symp Biomed Imaging. 2021 April ; 2021: 1827–1830. doi:10.1109/isbi48211.2021.9434114.

HISTOPATHOLOGY IMAGE REGISTRATION BY INTEGRATED TEXTURE AND SPATIAL PROXIMITY BASED LANDMARK SELECTION AND MODIFICATION

Pangpang Liu[*], **Fusheng Wang**[†], **George Teodoro**[‡], **Jun Kong**[*,‡]

[*]Department of Mathematics and Statistics, Georgia State University, Atlanta, GA, 30303, USA

[†]Department of Computer Science, Stony Brook University, Stony Brook, NY, 11794, USA

[‡]Department of Computer Science, Federal University of Minas Gerais, Belo Horizonte, 31270, Brazil

[‡]Department of Computer Science, Emory University, Atlanta, GA, 30322, USA

Abstract

Three-dimensional (3D) digital pathology has been emerging for next-generation tissue based cancer research. To enable such histopathology image volume analysis, serial histopathology slides need to be well aligned. In this paper, we propose a histopathology image registration fine tuning method with integrated landmark evaluations by texture and spatial proximity measures. Representative anatomical structures and image corner features are first detected as landmark candidates. Next, we identify strong and modify weak matched landmarks by leveraging image texture features and landmark spatial proximity measures. Both qualitative and quantitative results of extensive experiments demonstrate that our proposed method is robust and can further enhance registration accuracy of our previously registered image set by 31.15% (correlation), 4.88% (mutual information), and 41.02% (mean squared error), respectively. The promising experimental results suggest that our method can be used as a fine tuning module to further boost registration accuracy, a premise of histology spatial and morphology analysis in an information-lossless 3D tissue space for cancer research.

Index Terms—

histopathology image registration; landmark evaluations; three-dimensional pathology

1. INTRODUCTION

The vast majority of prevalent tissue-based studies analyze two-dimensional (2D) histopathology images. However, such 2D projection representations are subject to significant information loss and bias. A promising solution is to extend such histology feature analysis to a three-dimensional (3D) tissue space [1, 2, 3]. As such a 3D microscopy

6.COMPLIANCE WITH ETHICAL STANDARDS

This is a numerical simulation study for which no ethical approval was required.

Author Manuscript Author Manuscript Author Manuscript Author Manuscript

image volume is made of serial tissue slides, an accurate spatial registration becomes the key premise of the 3D histopathology image analysis. Although there are numerous registration methods in the radiology field, such as the region-based diffeomorphic registration method [4], or the patch-based discrete registration algorithm [5], among others, the registration method for whole-slide histopathology images is scarce due to the giga-pixel image resolution. Additionally, histopathology tissues are often subject to global and local deformations during the slide preparation process, making histopathology image registration a challenging problem.

In our prior work, we have developed such a pioneering method that dynamically registers 3D subvolumes from serial gigapixel whole slide images by an optimal deformation estimation at low resolution, and a mapping and propagation method at the high resolution level [6]. Although such a method provides a feasible solution to the whole-slide histopathology image registration problem, its registration accuracy needs to be further improved to support the cell-level spatial alignment. To address this problem, we propose a registration method with integrated landmark processing by texture and spatial proximity measures in this study.

2. METHODS

Due to the strong variation in stains, we first normalize the slide color [8] and the pixel intensity. The resulting gray-scale images are used for registration by our previously published dynamic registration method [6]. We detect corner points based on Harris features [9] and nuclei [10] for landmark candidates. These candidates from the reference and target images are matched by normalized cross-correlation, and partitioned to strong and weak landmark pairs by the image texture similarity and local spatial proximity patterns. Strong matched landmarks serve as a reference to further adjust weak landmarks. With the resulting landmark pairs, the registered image is produced by pixel-wise local transformations from interpolation. The schema of our registration procedure is illustrated in Figure 1.

2.1. Landmark Extraction and Matching

For histology images with a clear presence of nuclei, we detect nuclei as landmarks by a convolutional neural network [10]. When it is challenging to detect nuclei, we choose to detect corner points as landmarks instead. To achieve a high registration accuracy, we impose the spatial locality constraint on matched landmarks from the reference and the target image. We denote (x^r, y^r) as a landmark coordinate in the reference image. The size of the square local neighborhood in the reference and target image is L^r and L^t (s.t. $L^r < L^t$), respectively. For each local square reference image patch $P^r = P(x^r, y^r, L^r)$ with center (x^r, y^r), we find landmark candidates from a larger local square region $P^t = P(x^r, y^r, L^t)$ in the target image. Our aim is to find a matched point (x^t, y^t) in P^t for each (x^r, y^r) in P^r. To obtain the initial matched point (x^t, y^t) in P^t, we find the maximum normalized cross-correlation c_{rt} between P^r and P^t. A correlation constraint is imposed to exclude weak correlation. The resulting initial matched point pair set is denoted as: $M_0 = \{\{(x^r, y^r), (x^t, y^t)\} : c_{rt} > \eta\}$, where η is the normalized cross-correlation threshold.

Author Manuscript Author Manuscript Author Manuscript Author Manuscript

Next, we differentiate strong from weak matched points in M_0 by the local distance pattern analysis. We first find n nearest landmarks (x_i^r, y_i^r), $i = 1, \ldots, n$ for each (x^r, y^r) and n nearest landmarks (x_i^t, y_i^t), $i = 1, \ldots, n$ for each (x^t, y^t) in M_0 by Euclidean distance, respectively. The resulting difference between the matched landmarks and the corresponding n nearest landmarks is denoted as:

$$\Delta_i^j = x^j - x_i^j, \Gamma_i^j = y^j - y_i^j, i = 1, \ldots, n, j = r, t$$

The selected matched landmarks are included in the following set subject to a local spatial constraint:

$$M_0^+ = \left\{ \left\{ (x^r, y^r), (x^t, y^t) \right\} : C_0(n) \right\}$$

where the constraint of the n spatial shifts is:

$$C_0(n) = \left\{ \Delta_i^r \Delta_i^t \geq 0, \left| \Delta_i^r - \Delta_i^t \right| < \tau \left| \Delta_i^r \right|, \Gamma_i^r \Gamma_i^t \geq 0, \left| \Gamma_i^r - \Gamma_i^t \right| < \tau \left| \Gamma_i^r \right|, \forall i = 1, \ldots, n \right\} \quad (1)$$

Note τ is the relative distance difference ratio cutoff. To obtain strong matched landmarks, we find m nearest landmarks for each landmark in M_0^+, and further generate a new matched landmark set M^+ subject to the distance constraint $C_0(m)$ described by Equation (1). We present such strong matched landmarks in a representative reference and target image in Figure 2.

2.2. Spatial Shift Modification

To further increase the registration accuracy, we next improve the spatial shifts of weak matched landmark pairs based on the spatial shifts of strong matched landmarks in proximity. For each matched landmark in $M_0^- = M_0 \backslash M^+$, we find the nearest landmark from M^+. We denote the set of shortest distances as $D_n = \left\{ d_r : \min_{(x^+, y^+) \in M^+} d_r^+ \right\}$, where d_r^+ is the Euclidean distance of a landmark from M_0^- and its counterpart in M^+. We define $d_{max} = \sup D_n$, and $d_{min} = \inf D_n$. The resulting set of matched landmarks after adjustment is $M_1^- = \left\{ \left\{ (x^r, y^r), (x^t, y^t) \right\} : x^t = x^r + dx, y^t = y^r + dy \right\}$, where $dx = w\left(x_r^+ - x_t^+\right) + (1 - w)\left(x^r - x^t\right)$, $dy = w\left(y_r^+ - y_t^+\right) + (1 - w)\left(y^r - y^t\right)$ and the non-linear weight w is $\max\left(0, e^{-\frac{d_r - d_{min}}{d_{max} - d_{min}}} - 0.5\right)$.

2.3. Selection by Texture and Spatial Proximity

Next, we find the nearest landmark in M^+ for each landmark in M_1^-, and further generate a new matched landmark set M_2^- subject to the distance constraint $C_0(1)$ by Equation (1). We extract SURF features of small reference and target local patches centered on each pair of landmarks in M_2^-, respectively. The resulting feature distance s_r is computed. As the spatial

Author Manuscript Author Manuscript Author Manuscript Author Manuscript

distribution of matched landmarks affects the end registration accuracy, we would like to have such matched landmarks distributed over the complete tissue image domain. Therefore, we design a dynamic feature distance cutoff value that depends on the local landmark spatial proximity: $\gamma = 0.1e^{-1/d_r^-}$, where d_r^- is the distance between the reference landmark from M_2^- and its closest neighboring reference landmark from M_2^-. The resulting landmark set is $\{M^- = \{\{(x^r, y^r), (x^t, y^t)\} : s_r < \gamma\}$, where s_r is the distance between the matched SURF features [7]. We assemble the final set of matched landmarks as $M^* = M^+ \cup M^-$. With matched points in M^*, pixel-wise spatial shift vectors are computed by interpolation.

Algorithm 1 Registration Mapping and Improvement

Input: $\{R, T\}$: A reference and target image pair
Output: $\overline{T}$: A registered image

Extract landmark candidates $\{(x_i^r, y_i^r), (x_i^t, y_i^t)\}$
Generate image patches $\{P_i^r, P_i^t\}, i = 1, 2, ..., N$
for $i \in (1, 2, ..., N)$ **do**
    if $c_{rt} > \eta$ **then** $M_0 \leftarrow \{(x_i^r, y_i^r), (x_i^t, y_i^t)\}$
for $(\{(x_i^r, y_i^r), (x_i^t, y_i^t)\} \in M_0$ **do**
    if $C_0(n)$ **then** $M_0^+ \leftarrow \{(x_i^r, y_i^r), (x_i^r, y_i^t)\}$
for $(\{(x_i^r, y_i^r), (x_i^t, y_i^t)\} \in M_0^+$ **do**
    if $C_0(m)$ **then** $M^+ \leftarrow \{(x_i^r, y_i^r), (x_i^r, y_i^t)\}$
for $(\{(x_i^r, y_i^r), (x_i^t, y_i^t)\} \in M_0^- = M_0 \setminus M^+$ **do**
    $x_i^t = x_i^r + dx_i, y_i^t = y_i^r + dy_i$
    $M_1^- \leftarrow \{(x_i^r, y_i^r), (x_i^t, y_i^t)\}$
for $(\{(x_i^r, y_i^r), (x_i^t, y_i^t)\} \in M_1^-$ **do**
    if $C_0(1)$ **then** $M_2^- \leftarrow \{(x_i^r, y_i^r), (x_i^t, y_i^t)\}$
for $(\{(x_i^r, y_i^r), (x_i^t, y_i^t)\} \in M_2^-$ **do**
    if $s_r < \gamma$ **then** $M^- \leftarrow \{(x_i^r, y_i^r), (x_i^t, y_i^t)\}$
$M^* = M^+ \cup M^-$
$\overline{T} \xleftarrow[\text{interpolate}]{M^*} T$

3. EXPERIMENT AND RESULTS

We test our registration fine-tuning method with 28 pairs of serial histopathology images of Hematoxylin and Eosin stained glioblastoma (GBM) biopsy sections. Although this set of images (3544 × 4096 pixel each) has been pre-aligned by our prior method [6], further spatial fine tuning is required. For our experiments, we set = 0.25, $L^r = 200$, $L^t = 500$, $\tau = 0.1$, $n = 4$, and $m = 2$.

To quantitatively evaluate the registration enhancement effect, we compute Correlation (COR), Mutual Information (MI), and Mean Squared Error (MSE) for each serial image pair. Our method enhances registration quality in all 28 image pairs. We also compare our method with state-of-the-art method pTV [11] and Demons [12, 13], with results shown in Table 1. Our method is consistently superior to pTV by all metrics for all 28 image pairs, and better than Demons in the vast majority of cases (24, 19, and 23 out of 28 image pairs by COR, MI, and MSE). Compared with results before registration, our method, on average, improves 31.15%, 4.88%, and 41.02% by COR, MI, and MSE, respectively. By contrast, pTV improves on average by 3.06% (COR), −0.76% (MI), and 7.89% (MSE), while

Author Manuscript Author Manuscript Author Manuscript Author Manuscript

Demons method presents 11.70% (COR), 2.74% (MI), and 16.50% (MSE) improvement on average.

In addition to quantitative measures, we illustrate the checkerboard views of representative results for visual comparisons in Figure 3. In our method, detected nuclei serve as landmark candidates for the top image, while Harris points are used in the bottom image. It is visually noticeable that certain tissue areas misaligned before our analysis become well aligned after our registration fine-tuning process. By contrast, neither pTV nor Demons method significantly improves registration quality. Such difference in image alignment is clearly manifested by insets in Figure 3. We further demonstrate the resulting 3D tissue volume composed with serial registered images by our method in Figure 4.

Furthermore, we validate our method with simulated images. We produce 100 random affine transformations with affine matrix entries subject to the uniform distribution $U(0, 0.5)$ and artificially warp a randomly selected GBM image by such transformations for distortion simulation. Next, we apply our proposed registration method to the resulting simulated deformed images. The registration enhancement quality measured by MI, COR, and MSE are computed and demonstrated in Figure 5 from top to bottom. The x-axis represents the deformed image index and the y-axis presents the numeric value of these measures before and after registration. It is clear that our method consistently improves registration quality in all experiments by all measures. When compared with pTV and Demons, our method performs better for all simulated image pairs by COR, and for the vast majority of simulated image pairs by MI (81, and 91 out of 100 image pairs) and MSE (71, and 98 out of 100 image pairs).

4. CONCLUSION

We have developed a pathology image registration fine-tuning method that evaluates and improves landmark candidates by integrated texture and spatial proximity measures. We partition the matched landmarks into strong and weak matched pairs. By modification and selection of weak matched pairs, we improve estimation of spatial shifts derived from weak matched landmark pairs. Therefore, the resulting registration accuracy is substantially enhanced. Both quantitative and visual evaluation results demonstrate the effectiveness of our method for fine tuning pathology image registration.

ACKNOWLEDGEMENT

This research is supported in part by grants from National Institute of Health 1U01CA242936, 5R01EY028450, R01CA214928, and National Science Foundation ACI 1443054 and IIS 1350885, and CNPq. There is no conflicts of interest to disclose.

7. REFERENCES

[1]. Liang Y, F.S., Treanor D, Magee D, Teodoro G, Zhu YY, Kong J, ”Liver whole slide image analysis for 3D vessel reconstruction,” Int. Symp. on Biomed. Imaging: From Nano to Macro, pp. 182–185, 2015.

[2]. Liang Y, Wang FS, Treanor D, Magee D, Teodoro G, Zhu YY, Kong J, ”A 3D primary vessel reconstruction framework with serial microscopy images,” Int. Conf. on MICCAI, pp. 251–259, 2015.

Author Manuscript Author Manuscript Author Manuscript Author Manuscript

[3]. Liang Y, Wang FS, Zhang PY, Saltz J, Brat DJ, Kong J, ”Development of a frame work for large scale three-dimensional pathology and biomarker imaging and spatial analytics,” AMIA Summits on Transl. Sci, pp. 75–84, 2017.

[4]. He H, Razlighi Q, ”Volumetric Registration of Brain Cortical Regions by Automatic Landmark Matching and Large Deformation Diffeomorphisms,” Proceedings of IEEE Int. Symp. on Biom. Imag, pp.1412–1417, 2020.

[5]. Dalca AV, Bobu A, Rost NS, Golland P, ”Patch-Based Discrete Registration of Clinical Brain Images,” Patch Based Tech Med Imaging, vol.9993, pp.60–67, 2016.

[6]. Rossetti BJ, Wang FS, Zhang PY, Teodoro G, Brat DJ, Kong J, ”Dynamic registration for gigapixel serial whole slide images,” in IEEE International Symposium on Biomedical Imaging, pp. 424–428, 2017.

[7]. Bay H, Ess A, Tinne T, Gool LV, ”SURF: Speeded Up Robust Features”, Computer Vision and Image Understanding, 110:346–359, 2008.

[8]. Macenko M, Niethammer M, Marron JS, Borland D, Woosley JT, Guan X, Schmitt C, Thomas NE, ”A Method for Normalizing Histology Slides for Quantitative Analysis”, IEEE International Symposium on Biomedical Imaging, pp. 1107–1110, 2009.

[9]. Harris C, Stephens M, ”A Combined Corner and Edge Detector”, Proceedings of the 4th Alvey Vision Conference, pp. 147–151, 1998.

[10]. Wang S, Wang T, Yang L, Yang DM, Fujimoto J, Yi F, Luo X, Yang Y, Yao B, Lin S, Moran C, Kalhor N, Weissferdt A, Minna J, Xie Y, Wistuba II, Mao Y, Xiao G, ”ConvPath: A Software Tool for Lung Adenocarcinoma Digital Pathological Image Analysis Aided by Convolutional Neural Network”, EBioMedicine, vol.50:103–110, 2019. [PubMed: 31767541]

[11]. Gigengack F, Ruthotto L, Burger M, Wolters CH, Jiang X, Schäfers KP, ”Motion Correction in Dual Gated Cardiac PET Using Mass-Preserving Image Registration”, Trans. on Med. Imag, 31(3):698–712, 2012.

[12]. Jean-Philippe Thirion J. p., “Image matching as a diffusion process: an analogy with maxwell’s demons”, Med. Im. Anal, 2(3):243–260, 1998.

[13]. Vercauteren T, Pennec X, Perchant A, Ayache N, ”Diffeomorphic Demons: Efficient Non-parametric Image Registration”, NeuroImage. 45(1):61–72, 2009.

Author Manuscript Author Manuscript Author Manuscript Author Manuscript

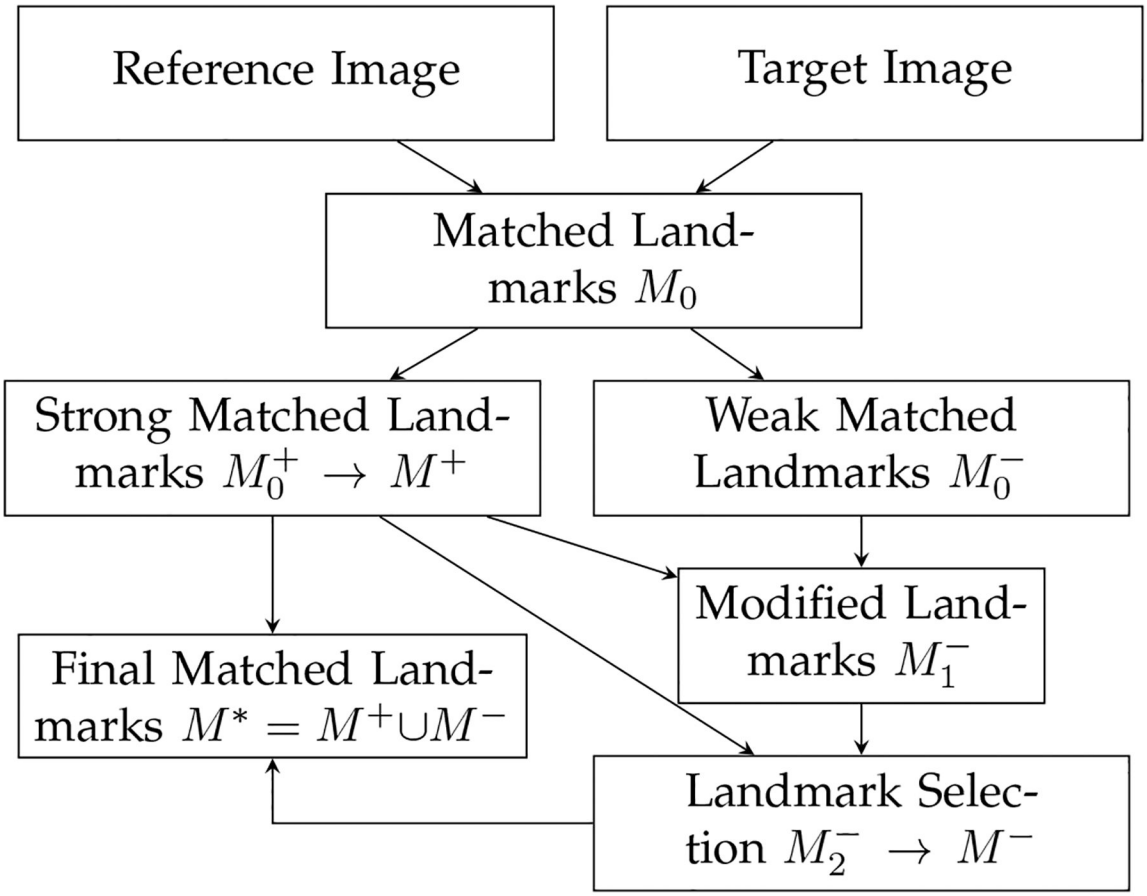

Fig. 1.
Schema of the proposed registration method with landmark selection and modification by the integrated use of texture and spatial proximity measures.

Author Manuscript Author Manuscript Author Manuscript Author Manuscript

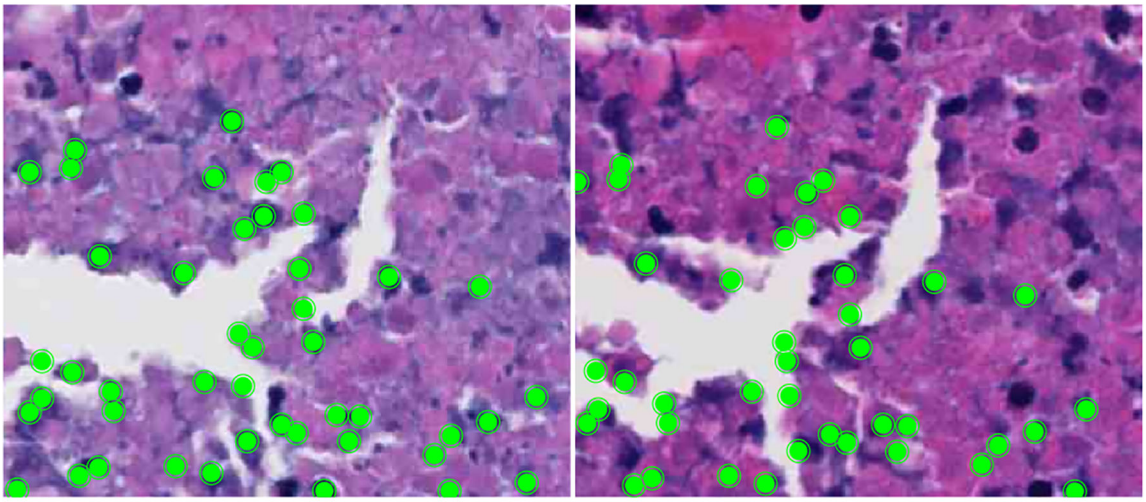

Fig. 2.
Strong matched landmarks are overlaid on a representative (Left) reference, and (Right) target image.

Author Manuscript Author Manuscript Author Manuscript Author Manuscript

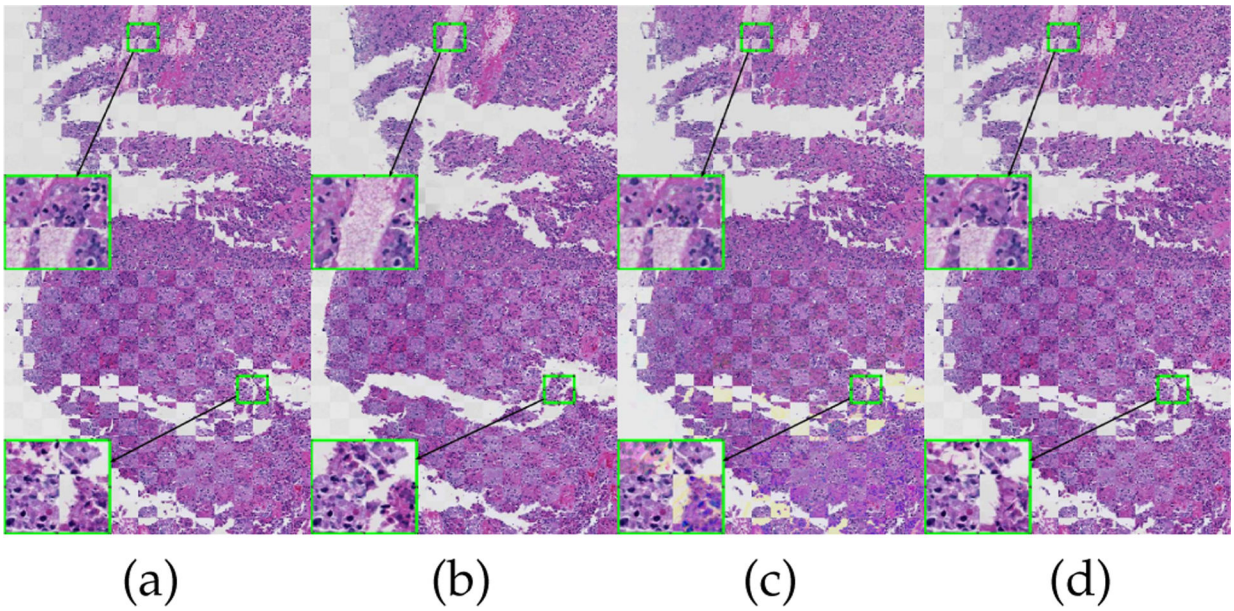

Fig. 3.

We present checkerboard views of representative registration results (a) before, after (b) our registration method with (top) nuclei and (bottom) Harris points serving as landmark candidates, (c) pTV, and (d) Demons method.

Author Manuscript Author Manuscript Author Manuscript Author Manuscript

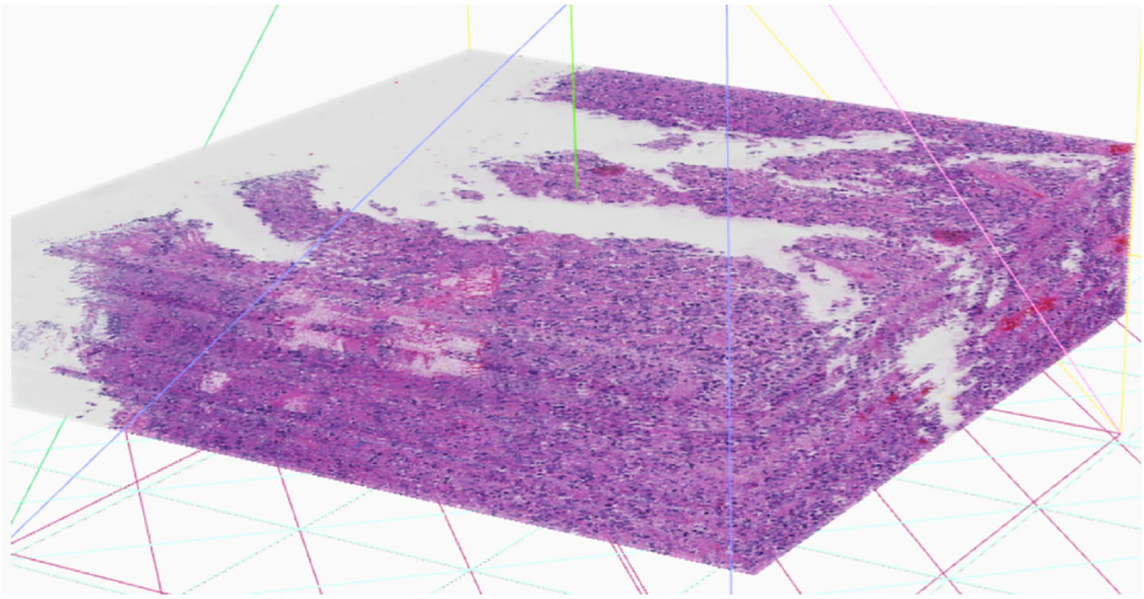

Fig. 4.
A 3D tissue volume composed with serial pathology image regions registered by our method.

Author Manuscript Author Manuscript Author Manuscript Author Manuscript

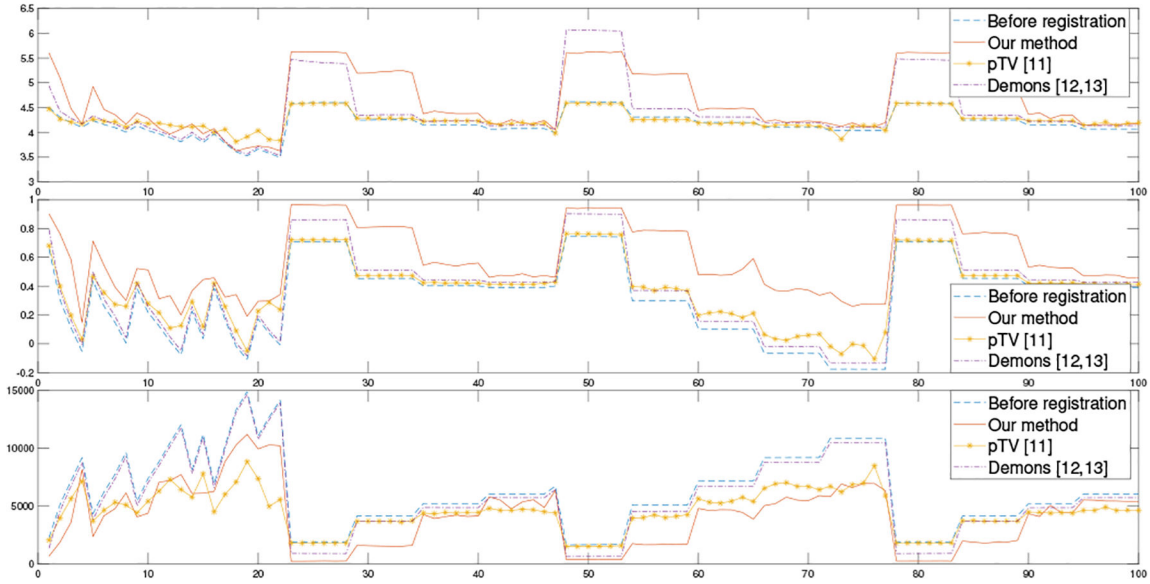

Fig. 5.

Registration improvement assessed by MI, COR, and MSE are presented from top to bottom.

Author Manuscript

Author Manuscript

Author Manuscript

Author Manuscript

Table 1.

Comparisons of registration quality assessed by different metrics.

	Before registration			After our method			pTV [11]			Demons [12, 13]		
N	**COR**	**MI**	**MSE**	**COR**	**MI**	**MSE**	**COR**	**MI**	**MSE**	**COR**	**MI**	**MSE**
1	0.616	4.381	2193	**0.767**	**4.540**	**1334**	0.635	4.363	2031	0.719	4.531	1588
2	0.656	4.361	2046	**0.771**	4.477	1359	0.679	4.336	1840	0.769	**4.537**	**1354**
3	0.389	4.139	3500	**0.767**	**4.459**	**1393**	0.402	4.063	3310	0.469	4.218	3026
4	0.628	4.213	2114	**0.756**	4.341	**1416**	0.650	4.148	1937	0.732	**4.356**	1516
5	0.623	4.275	2459	**0.754**	**4.439**	**1689**	0.652	4.180	2112	0.703	4.390	1941
6	0.620	4.291	2053	**0.776**	**4.464**	**1229**	0.637	4.260	1917	0.725	4.461	1475
7	0.404	4.244	3585	**0.724**	**4.588**	**1851**	0.423	4.275	3273	0.471	4.303	3145
8	0.651	4.402	2224	**0.777**	4.552	**1417**	0.673	4.390	2017	0.755	**4.572**	1544
9	0.648	4.179	1963	**0.777**	4.319	**1251**	0.664	4.188	1833	0.767	**4.376**	1282
10	0.637	4.303	1996	**0.770**	**4.455**	**1272**	0.660	4.222	1831	0.739	4.449	1420